ISSN: 2634-9221
European Journal of Applied Sciences; Vol. 14 No. 01 (2026) (656-666)
https://doi.org/10.14738/aivp.1401.19987

The Investigation on Multi-stage Cold Forming Process for Manufacturing of SCM435 Alloy Steel Spherical Joints

Chih-Cheng Yang[1], Chun-Yi Huang[2], & Shih-Chiang Wang[2]

1. Department of Mechanical and Automation Engineering, Taiwan Steel University, Taiwan
2. Graduate School of Mechatronic Science and Technology, Taiwan Steel University, Taiwan

Abstract: Multi-stage cold forming is commonly used for forging fasteners and parts. This study numerically simulates the five-stage cold forming process of SCM435 alloy steel spherical joints. The five-stage cold forming process includes preparation along with centering, upsetting, twice backward extrusions over a moving punch along with upsetting to spherical shape, and piercing. The numerical simulations of cold forming are carried out using the finite element code of DEFORM-3D. The formability of the workpiece is studied, such as the forming force response, maximum forming forces, effective stress and strain distributions, and metal flow pattern. In the five-stage forming process, the effective stress and effective strain of the workpiece are significantly increased due to the large deformation in the two forming stages of backward extrusion along with upsetting to a spherical shape, and in the forming stage of piercing. The flow line distributions are also very complex, especially the flow lines in the piercing region around the inner wall of the hole are severely bent and highly compacted, eventually leading to fracture. In the fourth stage, the workpiece is secondly backward extruded along with upset, and the maximum axial forming force is the largest of the five stages. In the third stage of the firstly backward extrusion along with upset, the forming energy is the highest of the five stages due to the longer acted axial forming stroke. From the first stage to the last stage, the total maximum axial forming forces are 2,209.5 kN and the total forming energies are approximately 4.60 kJ.

Keywords: multi-stage cold forming, spherical joints, formability, forming force, effective stress and strain distributions.

1. INTRODUCTION

Multi-stage cold forming is extensively to produce various part products, especially in the manufacture of fasteners and special parts [1]. The billet is formed sequentially through multiple stations at high speed. Generally, high mechanical properties, good surface appearance and precision are achieved without further processing. In cold forming processes, the prediction of forming forces and stresses is crucial for the design of punches and dies, as well as the selection of forming equipment. Numerical simulations are used in many cold forming applications to predict and analyze forming designs. Altan and Knoerr [2] used the two-dimensional finite element method to study suck-in extrusion defects, bevel gear forging, stress analysis of forging tools and multi-stage cold forging design. Lee et al. [3] used the rigid-plastic finite element method to design a multi-stage cold forging process for forming a constant-velocity joint housing with shaft. They studied the velocity distribution, effective strain distribution, and forging load, which are useful information in process design. Joun et al. [4] proposed a numerical simulation technique for the forging process with a spring-attached die. A penalty rigid-viscoplastic finite element method was used with an iterative force balance method to explore the importance of metal flow lines on quality

control and the influence of spring-attached dies on metal flow lines and the reduction of forming load. Roque and Button [5] used commercial FE code ANSYS to model forming operations and developed models to simulate ring compression tests and upsetting operations, a stage in the manufacturing process of automotive starter parts. Cho et al. [6] carried out a numerical investigation on the process design of axisymmetric parts in forward and backward extrusion during cold forging operations. The numerical simulation results were in good agreement with the experimental results.

Hu and Wang [7] proposed a multi-stage upsetting method to form a thick and wide flange at the pipe end. They analyzed the numerical simulation results and explored the method for determining the step length. Park et al. [8] applied the finite element method to establish a systematic process analysis method for the multi-stage forming of the constant velocity joint outer ring and to numerically analyze the formability of the multi-stage forming process. Farhoumand and Ebrahimi [9] used the finite element code ABAQUS to analyze the forward-backward-radial extrusion process and studied the effects of geometric parameters as well as process conditions on the process. The numerical results were compared with experimental data in terms of forming loads and material flow lines in different regions. They also used the hardness distribution of the longitudinal section of the product to verify the strain distributions obtained by numerical analysis. Ji et al. [10] applied the numerical code of DEFORM_2D to study the cold-forming mechanism of a five-stage extrusion process of shaft parts that were used in gearboxes. The results showed that the cold extrusion of the five-stage process was feasible and the forming rules were obtained. Paćko et al. [11] proposed an application of finite element analysis in the prediction and optimization of bolt forming process. The bolt forming process of six stages was studied, including shearing, three upsetting stages, backward extrusion, and trimming. They proposed and analyzed several tool modifications using numerical simulation. Kang and Ku [12] conducted a series of experimental studies on the multi-stage cold-forming process with spheroidized SCr420H billets. The results showed that the proposed multi-stage cold forging process resulted in that the outer race was well formed and the dimensional accuracy of the cold-formed outer race met the demands. Yang and Lin [13] conducted numerical and experimental studies on two forming modes of two-step extrusion of AISI 1010 carbon steel. The numerical results of effective strain distributions were consistent with the experimentally measured hardness distributions.

Ku [14] proposed a two-stage cold forging process for manufacturing AISI 1035 steel drive shafts with internal spline and spur gear geometry. This process mainly involved a forward extrusion for preform and a forward-backward extrusion for the drive shaft. The preform and the drive shaft produced by the two-stage cold forging experiments were compared with the required target and the numerically predicted configurations. The results showed that the proposed two-stage cold forging process could be well applied to the production of the drive shaft with internal spline and spur gear structures. Obiko et al. [15] used DEFORM 3D to perform three-dimensional finite element analysis to investigate the plastic deformation behavior of X20CrMoV121 steel during forging process. They studied the effect of forging temperature on the strain, stress and particle flow velocity distribution during forging process. Byun et al. [16] conducted a numerical study on the automatic multi-stage cold-forging of SUS304 stainless steel ball studs. They investigated the plastic deformation behavior of SUS304 stainless steel in the range of room temperature to 400 °C and used a general method to express the flow stress as a closed-form function of strain,

strain rate and temperature. This method performed best under high strain, especially in the multi-stage cold forging process. Jo et al. [17] developed a multi-stage cold forging process using finite element analysis to produce a high-strength one-body input shaft with a long body and no separate components. This study provided a proof-of-concept to design and develope a multi-stage cold forging process for producing one-body input shaft with improved mechanical properties and material recovery. Lee et al. [18] proposed using a multi-stage cold forging process to reduce the manufacturing cost of the solenoid valve while satisfying dimensional accuracy and performance. The forming process is divided into six stages to improve the dimensional accuracy of the armature outer diameter, overall length and slot portion.

Yang and Liu [19] conducted numerical and experimental studies on a multi-stage cold forming process of AISI 1010 steel relief valve regulating nuts. The forming force growth tendency obtained by numerical simulation was consistent with the experimental results. The effective strain distributions were consistent with the measured hardness distributions. The highly compact grain flow lines also led to higher hardness. Yang et al. [20] conducted a numerical study on the multi-stage cold forming process for manufacturing AISI 1022 carbon steel eccentric parts. The formability of the workpiece was numerically investigated. Although the total maximum axial forging load of four-stage forming was less than that of five-stage forming, the maximum lateral forging force in the last stage of four-stage forming was almost 5 times that of the last stage of five-stage forming. The increase in the lateral forming force might lead to punch wear and damage. Winiarski et al. [21] proposed a method for forming flanges in hollow parts. The process consisted of an extrusion with two dies that moved in an opposite direction to the punches. This special kinematics of the tools made it possible to form two flanges simultaneously in a single tool pass. Yang et al. [22] conducted a numerical analysis of multi-stage cold forming process of AISI 316 stainless steel battery bolts. The cold forming process through five stages consisted of preparation and centering, backward extrusion over a die pin, twice upsetting operations, and square trimming. Due to the large amount of deformation, the effective stress and the effective strain in the head of the workpiece were significantly high. The flow line distributions were also very complex, especially in the trimming region of the head were severely bent, highly compacted, and eventually fractured due to excessive trimming.

In this study, the numerical simulation of a five-stage cold-forming process for the manufacture of SCM435 alloy steel spherical Joints is investigated. The forming process includes preparation along with centering, upsetting operation, two operations of backward extrusion over a moving punch along with upsetting spherical shape, and piercing along with upsetting. The numerical simulation of cold forming is conducted using the finite element code of DEFORM-3D. The forming load responses are calculated and effective stress, effective strain and the metal flow pattern at various deformation zones are analyzed.

2. MATERIALS AND METHODS

The manufacturing process of the spherical joint is designed as a five-stage cold forming process. A cold-forging quality SCM 435 alloy steel wire coil is used in the cold-forming analysis. The chemical composition of the alloy steel wire is shown in Table 1.

Table 1: Chemical composition of SCM 435 alloy steel wires (wt.%).

C	P	Mn	Si	Al	Cu	Ni	Cr	Mo
0.37	0.014	0.74	0.21	0.048	0.007	0.01	0.99	0.17

The numerical study of cold forming is conducted using the finite element code of DEFORM-3D. The material is first cut into the desired-length billet through plastic shearing. A short billet of ϕ18.1mm × L15.5mm is numerically cut by an open-shearing die and transfers to forming stations. The three-dimensional and cross-section views for initial billet and product parts of five stages are shown in Figure 1.

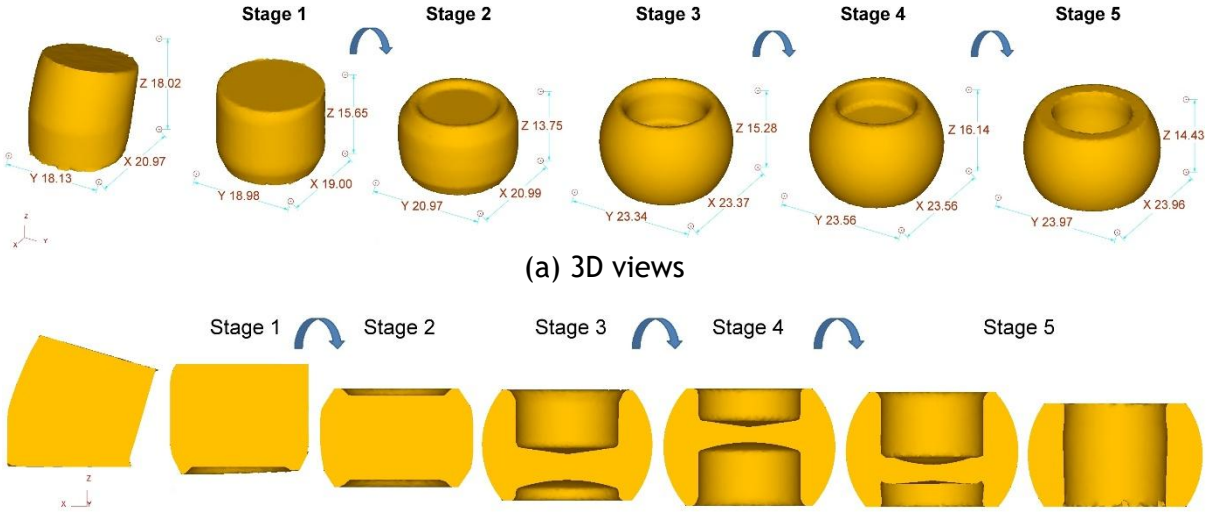

(a) 3D views

(b) cross-section views

Figure 1: The shapes for initial billet and product parts of each stage.

Due to cutting to length by open shearing, the whole cutoff billet is visibly deformed, as shown in Figure 1, which is obviously not an axisymmetric cylindrical body. For the first stage, as shown in Figures 1(a) and 1(b), the process includes flattening the billet and centering. Then, the workpiece is moved and simultaneously rotated to the second stage in which the workpiece is centering along with upset to diameter of ϕ21.0 mm. In the third stage, a cavity of ϕ14.1 mm is backward extruded to a depth of 7.0 mm over a moving punch at the upper end. Then, the workpiece is moved and simultaneously rotated to the fourth stage in which a cavity of ϕ14.1 mm is backward extruded at a depth of 5.0 mm over a moving punch at the upper end. Finally, the workpiece is moved and rotated again to the fifth stage in which the workpiece is pierced a hole along with upset to the specified dimensions by a moving punch. The deformation energy is

$$E = \int_0^{\Delta L} F dl \tag{1}$$

where F is forming force and ΔL is total acted forging stroke.

The numerical simulation of multi-stage cold forming is modeled as a 3D finite element analysis using DEFORM 3D. The workpiece is modeled using tetrahedral elements. The deformations of punches and dies are ignored and treated as rigid objects since their materials are usually much harder than the material of workpiece. The workpiece material

is a SCM 435 alloy steel billet which is considered as a rigid-plastic material with Von Misses yield criterion, isotropic hardening. To obtain more accurate simulation results, a cylindrical compression test, with the specimens of ϕ8.35mm × L11.41mm, is conducted in a 20 tonne universal testing machine under a constant ram speed of 3 mm/min at room temperature. The true stress and true strain are calculated using the following equations [23],

$$\sigma = P/A_0, \tag{2}$$

$$\varepsilon = (h - h_0)/h_0, \tag{3}$$

$$\sigma_t = \sigma\,(1 + \varepsilon) = \sigma\,(h/h_0), \tag{4}$$

$$\varepsilon_t = \ln(1 + \varepsilon) = \ln(h/h_0), \tag{5}$$

where σ is engineering stress, ε is engineering strain, P is compression force, A_0 is initial cross-sectional area, h_0 is initial height, h is the instantaneous height, σ_t is true stress and ε_t is true strain. Figure 2 shows the true stress-true strain diagram of SCM 435 alloy steel. The curve will be imported into the numerical code of DEFORM to conduct the forming simulation analysis.

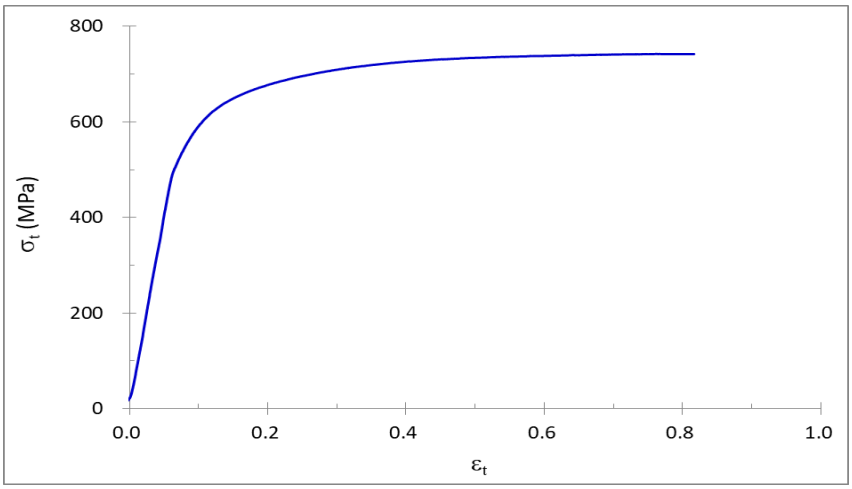

Figure 2: True stress-true train curve of SCM435 alloy steel by compression test.

The friction between the workpiece and tools is considered as constant shear friction, and the friction coefficient for cold forming is m = 0.12. The relevant simulation settings are listed in Table 2.

Table 2: Simulation parameters in the FE code of DEFORM.

Workpiece material	**SCM 435**
Workpiece/die property	Plastic/rigid
Temperature	20°C
Mesh number	38,000
Mesh element type	Tetrahedron
Friction model/friction coefficient	Constant shear friction/0.12

3. MULTI-STAGE COLD FORMING OF SPHERICAL JOINT

A five-stage numerical simulation study is conducted on the multi-stage cold forming process of the spherical joint. The effects of forming force responses, maximum forming loads, effective stress and strain distributions, and metal flow patterns are investigated.

3.1 The Forming Load Response and Deformation Energy

Figure 3 shows the axial force results of the five-stage cold forming simulation. The maximum forming forces are indicated for each stage. The acted axial forming stroke (ΔL) and deformation energy (E) for each stage are listed in Table 3.

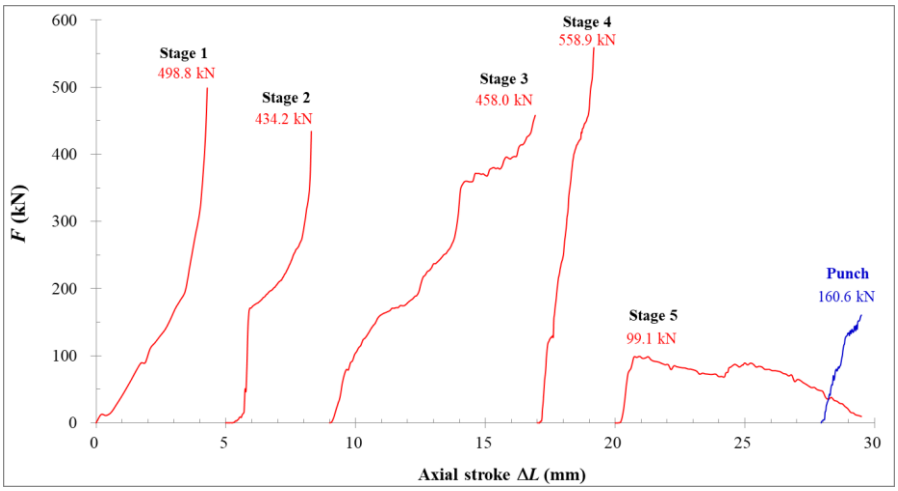

Figure 3: Axial Forging responses for five-stage forming.

Regarding the forming force responses at all stages, as shown in Figure 3, it is observed that in the first stage, the maximum axial forming force is 498.8 kN, which is the second largest among the five stages. The deformation in this stage is small to flatten the cutting edge of the billet and to center the end for the forming in the next stage. Thus, the acted axial forging stroke is 4.29 mm and the forming energy of 557.5 J is the smallest of the five stages, as shown in Table 3, due to the short axial forging stroke. In the second stage, the forming force decreases to a maximum of 434.2 kN, and the diameter of workpiece is slightly upset to ϕ21.0 mm (Figure 1). As shown in Table 3, the forming energy is 565.0 J, which is the second lowest among the five stages due to the shorter axial forming stroke (3.29 mm). In the third stage, the cavity with a diameter of ϕ14.1 mm is backward extruded at the upper end to a depth of 7.0 mm, while being upset into a spherical shape (Figure 1). The maximum forming force is 458.0 kN, which is the third largest among the five stages, as shown in Figure 3. The forming energy of 1,954.1 J is the largest due to the longer axial forming stroke of 7.92 mm, as shown in Table 3. In the fourth stage, a cavity with a diameter of ϕ14.1 mm is backward extruded from the upper end to a depth of 5.0 mm, with a maximum forming force of 558.9 kN, the highest among the five stages, as shown in Figure 3. The forming energy is 600.9 J, as shown in Table 3, with the shortest acted axial forming stroke of 2.18 mm. In the last stage, the workpiece is pierced a hole in a maximum forming force at 99.1 kN, and simultaneously upset to the specified dimensions by a moving punch in a maximum forming force at 160.6 kN, as shown in Figure 3. The forming energy is

634.8 J and the acted axial forming stroke of 9.49 mm is the longest among the five stages, as shown in Table 3, while the acted axial forming stroke of upsetting is only 1.55 mm and the forming energy is 142.0 J.

Table 3: The acted axial forging stroke (ΔL) and deformation energy (E) for each stage.

Stage	1	2	3	4	5 (Punch)	Total
E (J)	557.5	565.0	1,954.1	600.9	634.8 (142.0)	4,596.6
ΔL (mm)	4.29	3.29	7.92	2.18	9.49 (1.55)	

For the maximum axial forming force, as shown in Figure 3, the fourth stage, which the workpiece is the secondly backward extruded along with upset (Figure 1), is the largest among the five stages. For the forming energy, as shown in Table 3, the third stage, which a cavity is backward extruded at the upper end along with upset (Figure 1), is the largest among the five stages due to longer acted axial forming stroke. Overall, the total maximum axial forming forces from the first to the last stages are 2,110.4 kN; and the total forming energies shown in Table 3 are about 4.60 kJ.

3.2 The Effective Stress Analysis

The effective stress distributions at the final position of each stage for the five-stage forming are shown Figure 4 and the maximum effective stresses are indicated. For the first stage, stresses are arising at the upper and lower ends of workpiece when they are in contact with the dies, then the stresses increase as the forging load increases, the maximum effective stress is 757 MPa. It is observed that the effective stresses are highest at the upper and lower ends of the workpiece, as shown in Figure 4. However, the effective stresses are lowest in the upper right corner area due to the smaller deformation. For the second stage which involves slightly upset, the effective stresses are high in the upset deformation region. The maximum effective stress is 758 MPa. In the third stage which involves backward extrusion to a depth of 7.0 mm cavity at the upper end along with upsetting into a spherical shape, this causes the formation of a cavity at the upper face under high pressure resulting in an effective stress of up to 761 MPa on the workpiece and tool surfaces. The stress response in the whole workpiece is obviously larger, as shown in Figure 4. In the fourth stage, the process of backward extrusion over a moving punch is carried to form a depth of 5.0 mm cavity at upper face. This causes a large deformation in the head of workpiece under high pressure, generating high effective stress of up to 758 MPa, as shown in Figure 4.

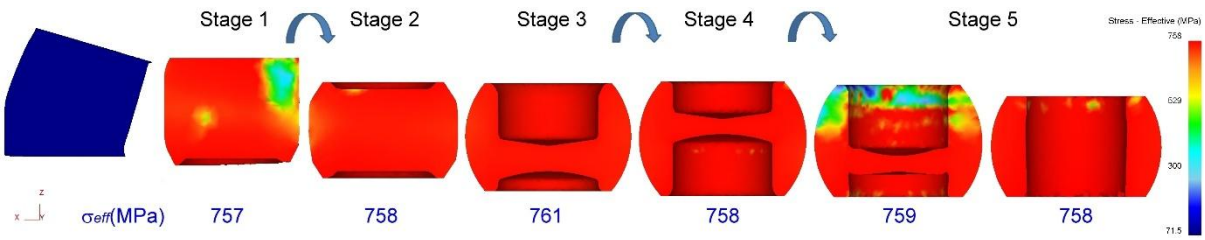

Figure 4: The effective stress distributions at the final position of each stage.

The stress response of the entire workpiece is obviously large. In the fifth stage, the process of piercing over a piercing punch is carried on to form a hole in the inner cavity and

simultaneously upsetting to the specified dimensions. Therefore, as shown in Figure 4, the stress response is relatively large in the piercing area of the workpiece, and so the upsetting region, resulting in effective stress as high as 758 MPa.

3.3 The Effective Strain Analysis

Figure 5 shows the effective strain distributions at the final position for the five stages. In the first stage, the effective strains in flatting and centering zones of workpiece are higher than the middle zone where the deformation is small. Due to the significant deformation of the cutoff billet by open shearing, the effective strain distribution is not symmetrical, as shown in Figure 5. For the second stage of slightly upsetting, the effective strains are high in the upper and lower ends, as shown in Figure 5. For the third stage of backward extrusion over a moving punch to a depth of 7.0 mm cavity at the upper end along with upsetting into a spherical shape, the effective strains are high in the upper end and the region of backward extrusion with large deformation, as shown in Figure 5. Due to the friction resistance on the contact surfaces between punch and workpiece, the region with higher effective strain increases along the punch. In the fourth stage, backward extrusion is conducted by a moving punch to form a cavity with a depth of 5.0 mm at the upper surface. As shown in Figure 5, the effective strain in the cavity interior region is higher, while the effective strain in other regions is relatively smaller. However, even though the first four stages are axisymmetric forming, the effective strain distribution is significantly asymmetrical, as shown in Figure 5, because the initial billet is not an axisymmetric cylindrical body. In the fifth stage, a moving punch is conducted to pierce a hole in the internal cavity and simultaneously upset to the specified dimensions. As shown in Figure 5, the effective strains are obviously high in the inner wall of the hole and in the piercing waste.

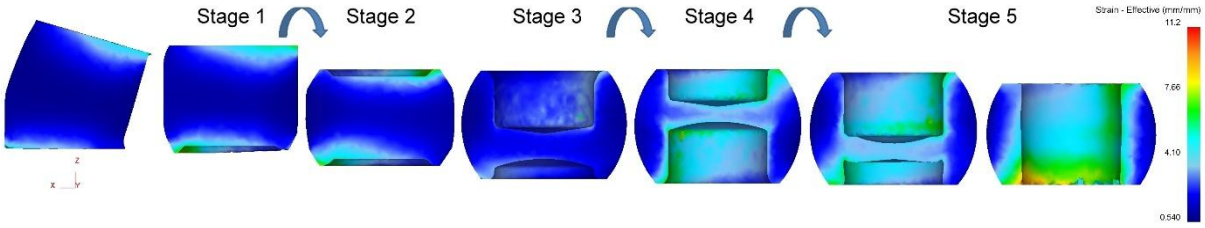

Figure 5: The effective strain distributions at the final position of each stage.

3.4 The Flow Line Analysis

The deformed grains and inclusions in the cold-formed metal are distributed in bands along the main deformation direction of the metal to form the grain flow lines. Figure 6 shows the simulation results of flow lines during the five-stage forming process. Due to the significant deformation of the cutoff billet under open shearing, the flow lines in the deformation area of the initial billet are curved but relatively uniformly distributed, as shown in Figure 6, except at both ends where the flow lines are vertically curved and highly compacted due to shear deformation. The compactness of the flow lines reflects the degree of hardness. Highly compacted flow lines indicate higher hardness in the metal [13,19].

In the first stage, the flow lines in flatting and centering regions of workpiece are highly compacted, as shown in Figure 6; while in the middle region with small deformation,

the flow line distributions almost remain uniform. For the second stage of slightly upsetting, the flow lines at both ends are obviously curved and highly compacted, as shown in Figure 6. In the third stage of backward extrusion over a moving punch at the upper end along with upsetting spherical shape, the flow lines in the inner wall of the upper cavity and in the cavity end area compression over extruding tools are bent and obviously highly compacted due to severe structural deformation, as shown in Figure 6. In the fourth stage of backward extrusion to form a cavity at the upper face, the flow lines in the extruding region and the end region of cavity compression over an extruding tool are severely curved and those in the end region between cavities are more highly compacted, as shown in Figure 6. For the last stage of piercing a hole in the internal cavity over a moving punch and simultaneously upsetting to the specified dimensions, the flow lines around the inner wall of the hole are severely curved, deformed and more highly compacted, eventually leading to fracture, as shown in Figure 6.

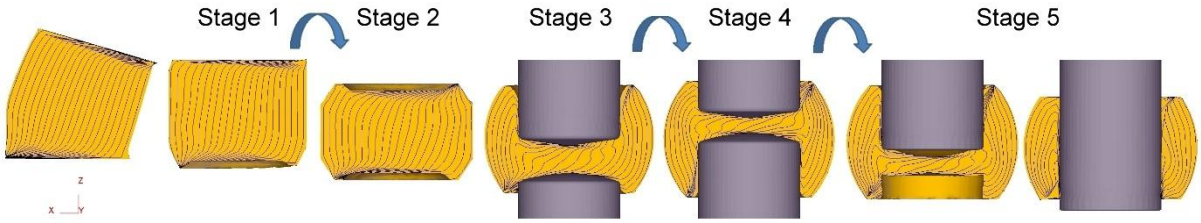

Figure 6: The simulation results of flow lines at the final position of each stage.

4. CONCLUSIONS

In this study, a numerical method is used to investigate the multi-stage cold forming process of SCM435 alloy steel spherical joints. The cold forming process through five stages includes flattening the billet and centering, upsetting operation, two operations of backward extrusion over a moving punch followed by upsetting into spherical shape, and piercing. The numerical simulations of cold forming process are performed using the FE code of DEFORM-3D. The formability of the workpiece is studied, such as forming force response, maximum forming force, effective stress and strain distributions, and metal flow pattern.

In the fourth stage, the maximum axial forming force of 558.9 kN is the highest of the five stages, which the workpiece is secondly backward extruded along with upset. However, in the third stage of the firstly backward extrusion along with upset, the maximum forming force of 458.0 kN is lower than in the fourth stage; while the forming energy of 1,954.1 J is the highest of the five stages due to the longer acted axial forming stroke. Overall, from the first stage to the last stage, the total maximum axial forming force is 2110.4 kN, and the total forming energy is approximately 4.60 kJ.

For the five-stage forming process, in the stages of backward extrusion forming over a moving punch to form the cavity along with upsetting, the effective stresses in the entire workpiece are significantly high, and the effective strains are also significantly high in the region of backward extrusion forming due to large deformation. In particular, the maximum effective stress in the third stage, the process of backward extrusion along with upsetting, is 761 MPa, which is the highest among the five stages. The flow line distributions are complex in which the flow lines in the regions of backward extruding a cavity and in the end region of cavities compression over extruding tools are severely curved and highly

compacted. Especially in the piercing region around the inner wall of the hole, the flow lines are severely bent and highly compacted, eventually leading to fracture. However, even if the forming stages are axisymmetric forming, the effective strain and flow line distributions are obviously not axisymmetric because the cutoff billet is significantly deformed through open shearing, resulting in a non-axisymmetric cylindrical body.

REFERENCES

[1]. Sevenler, K.; Raghupati, P.S.; Altan, T., Forming Sequence Design for Multi-stage Cold Forging. *Journal of Mechanical Working Technology*, 1987. 14(2): p.121-135.

[2]. Altan, T. and Knoerr, M., Application of the 2D Finite Element Method to Simulation of Cold Forging Processes. *Journal of Materials Processing Technology*, 1992. 35: p. 275–302.

[3]. Lee, J.-H.; Kang, B.-S.; Lee, J.-H., Process design in multi-stage cold forging by the finite-element method. *Journal of Materials Processing Technology*, 1996. 58(2-3): p.174-183.

[4]. Joun, M.S.; Lee, S.W.; Chung, J.H., Finite element analysis of a multi-stage axisymmetric forging process. *International Journal of Machine Tools and Manufacture*, 1998. 38: p. 843-854.

[5]. Roque, C.M.O.L. and Button, S.T., Application of the finite element method in cold forging processes. *Journal of the Brazilian Society of Mechanical Sciences*, 2000. 22(2): p. 189-202.

[6]. Cho, H.Y.; Min, G.S.; Jo, C.Y.; Kim, M.H., Process design of the cold forging of a billet by forward and backward extrusion. *Journal of Materials Processing Technology*, 2003. 135(2-3): p.375-381.

[7]. Hu, X.L.; Wang, Z.R., Numerical simulation and experimental study on the multi-step upsetting of a thick and wide flange on the end of a pipe. *Journal of Materials Processing Technology*, 2004. 151(1): p. 321–327.

[8]. Park, K.S.; VanTyne, C.J.; Moon, Y.H., Process analysis of multistage forging by using finite element method. *Journal of Materials Processing Technology*, 2007. 187–188: p. 586-590.

[9]. Farhoumand, A. and Ebrahimi, R., Analysis of forward–backward-radial extrusion process. *Materials & Design*, 2009. 30: p. 2152-2157.

[10]. Ji, D.S.; Jin, J.S.; Ma, W.J.; Xia, J.C.; Xia, H.G.; Dong, Y., Multistage Cold Extrusion Process and Forming Rules of Shaft Parts Used in Gearbox. *Advanced Materials Research*, 2010. 148-149: p. 683–687.

[11]. Paćko, M.; Sleboda, T.; Macioł, S.; Packo, P., Optimization of a Bolt Forming Process by Means of Numerical Simulation. *Steel Research International*, 2012.

[12]. Kang, B.S.; Ku, T.W., Experimental Study on Multi-Stage Cold Forging for an Outer Race of a CV Joint. *Transactions of Materials Processing*, 2014. 23: p.221–230.

[13]. Yang, C.-C. and Lin, X.-Y., The Forming Analysis of Two-stage Extrusion for 1010 Fastener. *Journal of Mechanical Engineering and Automation*, 2016. 6: p. 43-45.

[14]. Ku, T.-W., A Study on Two-Stage Cold Forging for a Drive Shaft with Internal Spline and Spur Gear Geometries. *Metals*, 2018. 8(11): 953.

[15]. Obiko, J.O.; Mwema, F.M.; Bodunrin, M.O., Finite Element Simulation of X20CrMoV121 Steel Billet Forging Process Using the Deform 3D Software. *SN Applied Sciences*, 2019. 1(9).

[16]. Byun, J.B.; Razali, M.K.; Lee, C.J.; Seo, I.D.; Chung, W.J.; Joun, M.S., Automatic Multi-Stage Cold Forging of an SUS304 Ball-Stud with a Hexagonal Hole at One End. *Materials*, 2020. 13: 5300.

[17]. Jo, A.R.; Jeong, M.S.; Lee, S.K.; Moon, Y.H.; Hwang, S.K., Multi-Stage Cold Forging Process for Manufacturing a High-Strength One-Body Input Shaft. *Materials*, 2021. 14(3): 532.

[18]. Lee, H.-S.; Park, S.-G.; Hong, M.-P.; Kim, Y.-S., Process design of multi-stage cold forging with small size for ESC solenoid valve parts. *Journal of Mechanical Science and Technology*, 2022. 36: p. 359-370.

[19]. Yang, C.-C. and Liu, C.-H., The Study of Multi-Stage Cold Forming Process for the Manufacture of Relief Valve Regulating Nuts. *Applied Sciences*, 2023. 13(10), 6299.

[20]. Yang, C.-C.; Sumampow, Y.; Cruz, S.N.D., The Cold Forming Analysis of Eccentric Parts. *European Journal of Applied Sciences*, 2023. 11(3): p. 407-421.

[21]. Winiarski, G.; Gontarz, A.; Skrzat, A.; Wójcik, M.; Wencel, S., Analysis of a New Process for Forming Two Flanges Simultaneously in a Hollow Part by Extrusion with Two Moving Dies. *Metals*, 2024. 14(6), 612.

[22]. Yang, C.-C.; Vien, T.T.T.; Lin, Y.-S., The Cold Forming Analysis of Stainless Battery Bolts. *European Journal of Applied Sciences*, 2025. 13(2): p. 72-83.

[23]. Hosford, W.F., *Mechanical Behavior of Materials*, Cambridge University, NY, USA, 2005.